BULLETIN OF THE GEOLOGICAL SOCIETY OF AMERICA
VOL. 60, PP. 1837-1856, 10 FIGS. DECEMBER 1949

SEISMIC EVIDENCE FOR THE FAULT ORIGIN OF OCEANIC DEEPS

BY HUGO BENIOFF

CONTENTS

	Page		Page
Abstract	1837	South American earthquake sequences	1846
Introduction	1837	Other deep-focus sequences	1855
Determination of strain-rebound increments	1838	Tsunamis and the great faults	1855
Tonga-Kermadec earthquake sequences	1841	References cited	1856

ILLUSTRATIONS

Figure	Page	Figure	Page
1. Strain-rebound increments of the Tonga-Kermadec shallow sequence ($h < 70$ km.)	1842	6. Strain-rebound increments of the South American shallow sequence ($h < 70$ km.)	1852
2. Strain-rebound increments of the Tonga-Kermadec deep sequence ($h = 70 - 480$ km.	1843	7. Strain-rebound increments of the South American intermediate sequence ($h = 70 - 300$ km.)	1853
3. Tonga-Kermadec fault mechanism suggested by strain-rebound curve of deep sequence	1843	8. Strain-rebound increments of the South American deep sequence ($h = 550 - 660$ km.)	1853
4. Tonga-Kermadec earthquakes and oceanic deeps	1844	9. South American earthquakes and oceanic deeps	1854
5. Sketch illustrating proposed origin of the great Tonga-Kermadec fault	1845	10. Sketch illustrating proposed origin of the great South American fault	1855

TABLES

Table	Page	Table	Page
1. Tonga-Kermadec shallow sequence	1839	4. South American intermediate sequence ($h = 70 - 300$ km.)	1849
2. Tonga-Kermadec deep sequence ($h = 70 - 680$ km.)	1840	5. South American deep sequence ($h = 550 - 660$ km.)	1851
3. South American shallow sequence ($h < 70$ km.)	1847		

ABSTRACT

A method is described for determining the elastic-rebound strain increments associated with earthquakes occurring on a particular fault. For a given sequence of earthquakes, a graph of the accumulated increments so determined plotted against time represents the actual fault movement during the interval covered by the sequence. The method also provides a means for determining whether or not a chosen sequence of earthquakes represents movements of a single fault structure. In this way it becomes possible to discover faults which otherwise may escape detection. Evidence of this kind is offered which indicates that the Tonga-Kermadec and South American sequences of earthquakes originate on great faults which dip under the continental masses. The faults are approximately 2500 km. and 4500 km. in length respectively. Their transverse dimensions are approximately 900 km. each. They both extend to a depth of approximately 650 km.—more than one tenth of the radius of the earth. The oceanic deeps associated with these faults are surface expressions of the downwarping of their oceanic blocks. The upwarping of their continental blocks have produced islands in the Tonga-Kermadec region and the Andes Mountains in South America.

INTRODUCTION

In another paper in preparation the writer develops a method for deriving numbers proportional to the elastic-rebound strain increments associated with individual earthquakes on a given fault. The method depends upon the instrumental earthquake magnitude scale

of Richter (1935) as revised by Gutenberg and Richter (1942). In a study of a number of aftershock sequences it has yielded information as to the strain activity of fault rocks during the time intervals in which aftershocks occurred. The strain characteristics so determined are in close agreement with the creep-recovery characteristics of rocks as measured in the laboratory. It was thus possible to demonstrate with reasonable certainty that aftershocks are produced by elastic afterworking of the fault rocks. The method has been applied to a study of sequences of earthquakes, other than aftershocks, originating in a number of active seismic regions. If the earthquakes of a given sequence are generated by strain-relief increments on a single fault, a graph of the accumulated increments plotted against time represents the actual intermittent motion of the fault blocks. The method thus makes it possible to observe tectonic processes in action. It may serve also to determine whether or not a given sequence of earthquakes is derived from movements of a single fault structure and so, in effect, to establish the existence of a fault which may have otherwise escaped detection. The discovery of two great faults from evidence of this kind is presented.

Determination of Strain-Rebound Increments

It will be of help to review briefly the procedure for deriving elastic strain-rebound increments from earthquake magnitudes. If an average elastic strain ϵ_1 preceding an earthquake is assumed to be distributed uniformly throughout an effective volume V of the *fault rock*, the strain energy stored in the rock is given by the equation:

$$E = \tfrac{1}{2}\mu V\epsilon_1^2. \qquad \text{ergs} \ldots\ldots (1)$$

where μ is the appropriate elastic constant of the rock. When the fault slips to produce the earthquake, a fraction p of the stored elastic energy is converted into seismic waves. Thus if J is the energy of the waves,

$$J = \tfrac{1}{2}P\mu V\epsilon_1^2. \qquad \text{ergs} \ldots\ldots (2)$$

For a given fault μ and V are constants. Moreover it is reasonable to assume that p is also constant and very nearly equal to unity. Hence equation (2) may be written

$$J = C^2\epsilon_1^2. \qquad \text{ergs} \ldots\ldots (3)$$

where C is a constant such that

$$C^2 = \tfrac{1}{2}p\mu V.$$

If the strain is reduced to zero during the earthquake the stored elastic strain is equal to the strain rebound, that is

$$\epsilon_1 = \epsilon$$

Hence

$$J = C^2\epsilon^2 \qquad \text{ergs} \ldots\ldots (4)$$

Taking the square root of equation (4),

$$J^{\frac{1}{2}} = C\epsilon \qquad (\text{ergs})^{\frac{1}{2}} \ldots\ldots (5)$$

Thus on a given fault the square root of the energy of an earthquake is proportional to the *elastic-strain rebound increment* which generates it. The fault-rebound displacement x corresponding with the strain-rebound increment ϵ is given by

$$x = m\epsilon$$

where m is a constant depending upon the size and shape of the volume V of strained rock. Hence

$$J^{\frac{1}{2}} = kx \qquad \ldots\ldots\ldots (6)$$

where $k = mC$. The square root of the earthquake energy is thus proportional to the rebound displacement also. If S is the accumulated sum of the values of $J^{\frac{1}{2}}$ for a sequence of earthquakes derived from a single fault, a graph of S versus time represents the fault displacement (multiplied by the undetermined constant k) or the strain relief (multiplied by C) as a function of time. Values for $J^{\frac{1}{2}}$ may be derived from Richter's instrumental magnitude M by means of the following equation which is derived by Gutenberg and Richter (1942)[1]:

$$\log J^{\frac{1}{2}} = 6.0 + 0.9\,M \qquad \ldots\ldots\ldots (7)$$

In the two sequences represented in this study, magnitudes, hypocenters, and origin

[1] The constants in equation (7) represent the authors' latest revised values. The probable error is $\pm \frac{1}{2}$ magnitude.

TABLE 1.—TONGA-KERMADEC SHALLOW SEQUENCE ($h < 70$ km.)

Date	J.D.	ϕ	λ	M	$J^{\frac{1}{2}} \times 10^{12}$	$S \times 10^{12}$
1910, June 29	2,418,852	32 S	176 W	7.0	2.0	2.0
1913, June 26	19,945	20	174	7.6	7.1	9.1
1917, May 1	21,350	29	177	8.0	16.0	25.1
1917, June 24	21,404	21	174	7.25	23.4	28.5
1917, June 26	21,406	15½	173	8.3	28.0	56.5
1917, Nov. 16	21,549	29	177½	7.5	5.6	62.1
1919, Apr. 17	22,066	29½	178	7.0	2.0	64.1
1919, Apr. 30	22,079	19	172½	8.3	28.0	92.1
1921, Feb. 27	22,748	18½	173	7.2	3.2	95.3
1924, Apr. 30	23,906	34	176	6.0	.2	95.5
1924, Aug. 10	24,008	30	178	6.75	1.2	96.7
1926, Mar. 16	24,591	16½	171	6.0	.2	96.9
1927, July 3	25,065	15	172½	6.25	.4	97.3
1929, Aug. 3	25,827	17	172½	6.5	.7	98.0
1930, Jan. 14	25,991	16	171	6.25	.4	98.4
1930, Feb. 14	26,022	21	175	6.5	.7	99.1
1930, Sept. 22	26,242	35½	179½	6.5	.7	99.8
1931, June 9	26,502	14	174	6.5	.7	100.5
1931, June 9	26,502	24½	176	6.25	.4	100.9
1931, Aug. 13	26,567	29	178	6.25	.4	101.3
1931, Nov. 18	26,664	20	174	6.0	.2	101.5
1932, Mar. 8	26,775	18½	179 E	6.25	.4	101.9
1932, Apr. 3	26,801	30¾	177½ W	6.25	.4	102.3
1932, May 22	2,426,850	20 S	174 W	6.25	.4	102.7
1933, Jan. 27	27,100	16	172	6.75	1.2	103.9
1933, Mar. 15	27,147	20	174	6.0	.2	104.1
1933, May 20	27,213	20	174½	6.0	.2	104.3
1933, June 18	27,242	15	172	6.0	.2	104.5
1933, July 24	27,278	16	173½	6.75	1.2	105.7
1934, Jan. 31	27,469	16	173½	6.25	.4	106.1
1934, Apr. 24	27,552	14	174	6.25	.4	106.5
1934, May 5	27,564	32	179	6.25	.4	106.9
1935, Feb. 4	27,838	20	174	6.25	.4	107.3
1935, Mar. 29	27,891	29	177½	6.25	.4	107.7
1935, Apr. 5	27,898	22	175	6.0	.2	107.9
1936, Mar. 20	28,248	14½	173½	6.25	.4	108.3
1936, Sept. 6	28,418	21½	174	6.0	.2	108.5
1939, Feb. 3	29,298	22½	175½	6.25	.4	108.9
1940, July 20	29,831	15½	173	6.0	.2	109.1
1940, Aug. 11	29,853	15½	172	6.0	.2	109.3
1940, Aug. 24	29,866	15½	173	6.0	.2	109.5
1941, Aug. 2	30,209	28½	178	7.1	2.5	112.0
1941, Sept. 16	30,254	28¾	177½	7.0	2.0	114.0
1941, Oct. 5	30,273	14½	173¾	6.5	.7	114.7
1942, Nov. 2	30,666	19	173	6.9	1.6	116.3
1942, Dec. 22	30,716	16¾	174	6.75	1.2	117.5
1943, June 3	2,430,879	16 S	173 W	6.5	.7	118.2
1943, Sept. 11	30,979	15	174	6.9	1.6	119.8
1943, Sept. 14	30,982	30	177	7.6	7.1	126.9
1943, Sept. 22	30,990	35½	178½	6.75	1.2	128.1
1943, Oct. 24	31,022	22	174	7.0	2.0	130.1
1943, Dec. 27	31,086	32	178½	6.25	.4	130.5
1943, Dec. 30	31,089	32½	177	6.25	.4	130.9
1946, Nov. 13	32,138	20	123½	7.5	5.6	136.5
1948, Sept. 9	32,804	21	174	8.0	16.0	152.5

TABLE 2.—TONGA-KERMADEC DEEP SEQUENCE (h = 70–680 km.)

Date	J.D.	ϕ	λ	M	$J^{\frac{1}{2}} \times 10^{12}$	$S \times 10^{12}$	h
1907, Apr. 1	2,417,667	18 S	177 W	7.25	3.30	3.30	400
1909, Feb. 22	18,361	18	179 W	7.5	5.60	8.90	550
1910, Apr. 21	18,784	20	177 W	7.0	2.00	10.90	330
1910, Aug. 21	18,906	17	179 W	7.25	3.30	14.20	600
1910, Dec. 15	19,022	21	178 W	7.0	2.00	16.20	600
1911, Apr. 29	19,157	27	179½ E	6.5	.70	16.90	600
1911, July 19	19,230	29	179 W	6.9	1.60	18.50	200
1911, Aug. 22	19,271	21	176 W	7.3	3.50	22.00	300
1912, May 15	19,539	30	178½ W	6.5	.70	22.70	250
1913, May 8	19,897	17	174½ W	7.0	2.00	24.70	200
1915, Feb. 26	20,556	20	180	7.25	3.30	28.00	600
1916, July 8	21,054	18	180	7.0	2.00	30.00	600
1918, May 22	21,737	17	177½ W	7.0	2.00	32.00	380
1918, Oct. 4	21,872	19	174 W	7.0	2.00	34.00	130
1919, Jan. 1	21,961	19½	176½ W	7.75	9.00	43.00	180
1919, Aug. 19	22,191	20½	178½ W	7.2	3.20	46.20	300
1922, Mar. 11	23,126	22	180	6.75	1.20	47.40	570
1924, Jan. 17	23,803	21	176 W	7.0	2.00	49.40	350
1924, May 5	23,912	21	178 W	7.3	3.50	52.96	560
1924, May 26	23,933	19	179 W	6.25	.42	53.32	550
1924, Dec. 27	24,148	21½	179 W	6.25	.42	53.74	540
1927, Apr. 2	24,974	20	177½ W	7.1	2.50	56.24	400
1928, June 17	2,425,416	21½ S	179½ W	6.25	.42	56.66	640
1928, Sept. 12	25,493	31	180	6.25	.42	57.08	500
1930, Apr. 30	26,098	20	176 W	6.75	1.20	58.28	180
1931, Apr. 4	26,437	20	179¾ W	6.75	1.20	59.48	680
1931, May 15	26,478	29	180	6.0	.20	59.68	500
1931, July 20	26,544	14	173 W	6.5	.70	60.38	80
1931, Oct. 18	26,634	26	180	6.75	1.20	61.58	500
1932, May 27	26,856	25½	179¼ E	7.75	9.00	70.58	600
1932, May 27	26,856	25½	179¼ E	6.5	.70	71.28	600
1932, May 27	26,856	25½	179¼ E	6.25	.40	71.68	600
1932, May 27	26,856	25½	179¼ E	5.75	.10	71.78	600
1932, June 17	26,877	20	176 W	6.0	.25	72.03	200
1932, July 21	26,911	27	178 W	6.5	.70	72.73	170
1932, Oct. 21	27,034	30	179 W	6.0	.25	72.98	70
1933, Jan. 24	27,098	21	180	6.25	.42	73.40	600
1933, May 21	27,246	35	180	6.0	.25	73.65	100
1933, June 12	27,267	22	176 W	6.5	.70	74.35	80
1933, Sept. 7	27,324	21½	179¾ W	7.1	2.50	76.85	600
1933, Nov. 8	27,386	30	177 W	5.5	.10	76.95	80
1934, Jan. 18	27,459	21	179 W	6.5	.70	77.65	580
1934, Feb. 10	27,480	20½	176½ W	6.5	.70	78.35	230
1934, Oct. 11	27,723	23½	180	7.3	3.50	81.85	540
1934, Sept. 23	27,735	30	177 W	6.0	.25	82.10	80
1934, Nov. 9	2,427,751	17½ S	174 W	6.25	.42	82.52	80
1934, Dec. 12	27,785	25	178 E	6.50	.70	83.22	600
1934, Dec. 16	27,789	23½	179½ W	6.9	1.60	84.82	530
1935, Jan. 2	27,806	17½	174½ W	7.1	2.50	87.32	300
1935, Apr. 20	27,914	31½	179½ W	5.75	.15	87.47	500
1935, July 16	28,001	20	178½ W	6.5	.70	88.17	580
1935, July 29	28,014	20¾	178 W	7.2	3.20	91.37	510

TABLE 2.—*Continued*

Date	J.D.	ϕ	λ	M	$J^{\frac{1}{2}} \times 10^{12}$	$S \times 10^{12}$	h
1935, Aug. 22	2,428,038	16	174 W	6.25	.42	91.79	100
1935, Sept. 13	28,060	20	179 W	6.0	.25	92.04	600
1936, Feb. 11	28,211	18½	178 W	6.75	1.20	93.24	570
1936, Apr. 7	28,267	21	177 W	6.0	.25	93.49	100
1936, Nov. 16	28,490	21	178 W	6.5	.70	94.19	540
1936, Nov. 26	28,500	18½	178 W	6.5	.70	94.89	560
1937, Apr. 16	28,641	21½	177 W	7.75	9.00	103.89	400
1937, May 11	28,666	26½	178 E	6.50	.70	104.59	640
1937, June 20	28,706	26½	178 E	6.25	.40	104.99	650
1937, Sept. 1	28,809	32	180	7.0	2.00	106.99	120
1938, Mar. 7	28,965	19	178 W	6.0	.25	107.24	500
1938, Apr. 15	29,004	33	179 E	5.75	.15	107.39	580
1938, Apr. 25	29,014	19	176½ W	5.5	.10	107.49	400
1938, May 16	29,035	27	179 E	5.75	.15	107.64	600
1939, May 22	29,406	22½	179 W	6.0	.25	107.89	600
1942, Jan. 1	2,430,361	20½ S	180	6.25	.42	128.11	630
1942, June 16	30,527	21½	179 E	6.75	1.20	129.31	550
1942, July 7	30,548	21	178 W	6.75	1.20	130.51	430
1942, Aug. 29	30,601	24	179½ E	6.75	1.20	131.71	570
1943, Mar. 4	30,788	22	179½ W	6.0	.25	131.96	600
1943, Mar. 24	30,808	23	179 W	6.25	.42	132.38	430
1943, Apr. 29	30,844	24½	180	6.5	.70	133.08	530
1943, May 12	30,868	20	175 W	5.75	.15	133.23	270
1943, May 29	30,874	21	179½ W	6.5	.70	133.93	630
1943, June 26	30,902	18	178 W	6.25	.42	134.35	550
1943, July 11	30,917	32½	178½ W	7.0	2.00	136.35	180
1943, Sept. 28	30,996	30	178 W	7.1	2.50	138.85	90
1944, Apr. 23	31,204	22	177½ W	6.5	.70	139.55	370
1944, May 14	31,225	23	179½ E	6.0	.25	139.80	600
1944, May 25	31,236	21½	179½ W	7.2	3.20	143.00	640
1944, July 11	31,283	19½	175½ W	6.75	1.20	144.20	180
1944, Aug. 26	31,329	18	175½ W	6.25	.42	144.62	240
1944, Oct. 11	31,375	15	173½ W	6.75	1.20	145.82	80
1944, Nov. 14	31,406	24½	179½ E	6.0	.25	146.07	610
1944, Nov. 30	31,425	23	179 W	6.75	1.20	147.27	180
1944, Dec. 1	31,426	21	178½ W	6.4	.60	147.87	600
1945, Nov. 26	31,786	21	180	7.0	2.00	149.87	600
1946, Aug. 21	32,054	24	177 W	7.0	2.00	151.87	100
1946, Sept. 26	2,432,090	25 S	179 E	7.0	2.00	153.87	600
1946, Oct. 8	32,112	25	178 E	6.75	1.20	155.07	670
1946, Nov. 28	32,154	18½	174 W	6.75	1.20	156.27	290
1946, Dec. 17	32,172	21	177 W	6.5	.70	156.97	580
1947, July 13	32,381	19	175 W	6.25	.42	157.39	120
1948, Jan. 27	32,578	20	178 W	7.25	3.30	160.69	600?

times were generously made available to me by Doctors Gutenberg and Richter from the manuscript of their book on *Seismicity of the Earth* (1949). The shallow-focus magnitudes were determined jointly by the two authors. The deep-focus magnitudes were determined by Gutenberg (1945) using the method he developed for this class of earthquake foci.

TONGA-KERMADEC SEQUENCES

The data for the Tonga-Kermadec sequences are given in Tables 1 and 2. The dates of origin have been converted into Julian days in order to simplify making of the graphs. In the tables t is the Julian day of origin, ϕ is the latitude of the epicenter, λ is the longitude of the

epicenter, h is the depth of focus in kilometers, and M is the magnitude. Figure 1 is a graph of S versus time for the shallow-earthquake sequence. Each circular dot represents the strain-relief increment of a single earthquake. The

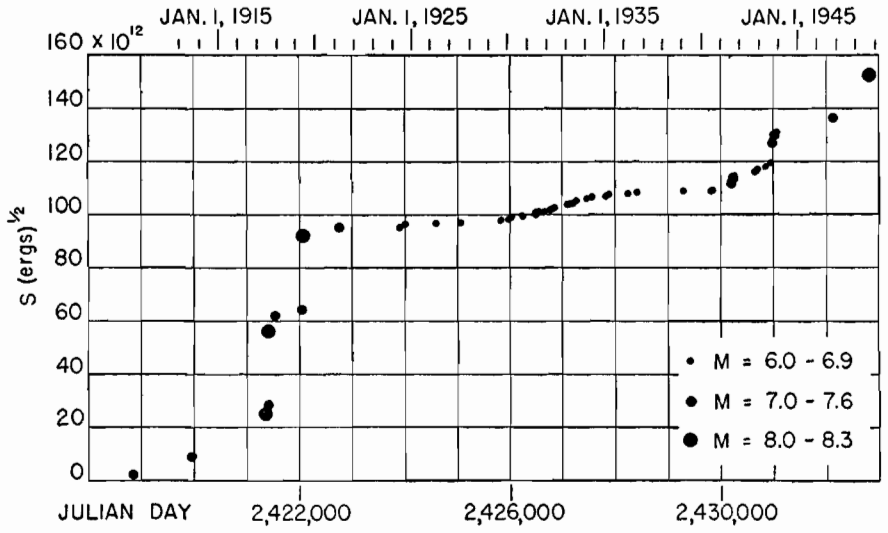

FIGURE 1.—STRAIN-REBOUND INCREMENTS OF TONGA-KERMADEC SHALLOW SEQUENCE (h < 70 km.) The plotted values are multiplied by the undetermined constant C of equation (5).

relation between the diameter of a dot and the magnitude of the earthquake with which it is associated is shown in the legend. This curve exhibits a rather large amount of irregularity—a characteristic found in a number of shallow sequences having large earthquakes. Presumably these sequences require greater time intervals than the present available maximum of 45 years of instrumental observations in order to show their characteristic trends. Figure 2 is a graph of S for the deep-focus sequence. This sequence includes all earthquakes of the region having focal depths greater than 70 km. which is taken to be the lower limit of the shallow earthquake sequence. The foci in this deep sequence are distributed uniformly to a depth of approximately 650 km. The curve of Figure 2 is made up of two phases. The graph of the first phase which ends at J.D. 2,426,634 (1931 October 18) was drawn from the calculated values of S in the equation

$$S_1 = [-257 + 79 \log t] \times 10^{12} \quad \ldots\ldots\ldots\ldots (8)$$

This equation represents a type of creep which has been observed in the laboratory for rocks (Griggs, 1939) and other solids (Lutts and Himmelfarb, 1940) subjected to constant compressional stress and which is designated elastic creep, since upon release of the stress the sample recovers completely—given enough time. In engineering literature, creep of this kind is considered a manifestation of strain hardening. The second phase begins with the great earthquake of 1932 May 26 and continues to the present date. The curve for this phase was calculated from the equation

$$S_2 = -87.7 \times 10^{12} + 16.1 \times 10^9 t \quad \ldots\ldots\ldots\ldots (9)$$

This equation represents a movement with constant velocity. The smoothness and singular shapes of the curves representing the two phases provide convincing evidence that the sequence of earthquakes which they represent must have been generated on a single fault. On this basis, the origin of the two phases can be explained by reference to the schematic fault diagram shown in Figure 3. It is assumed that the fault surfaces were subject to stress in the directions shown by the arrows. The corresponding indentations and elevations A, B, C, D represent points or areas over which the fault surfaces were locked. When the stress at any one of these points exceeded the locking strength, faulting took place. In this way each point became in turn the focus of one of the

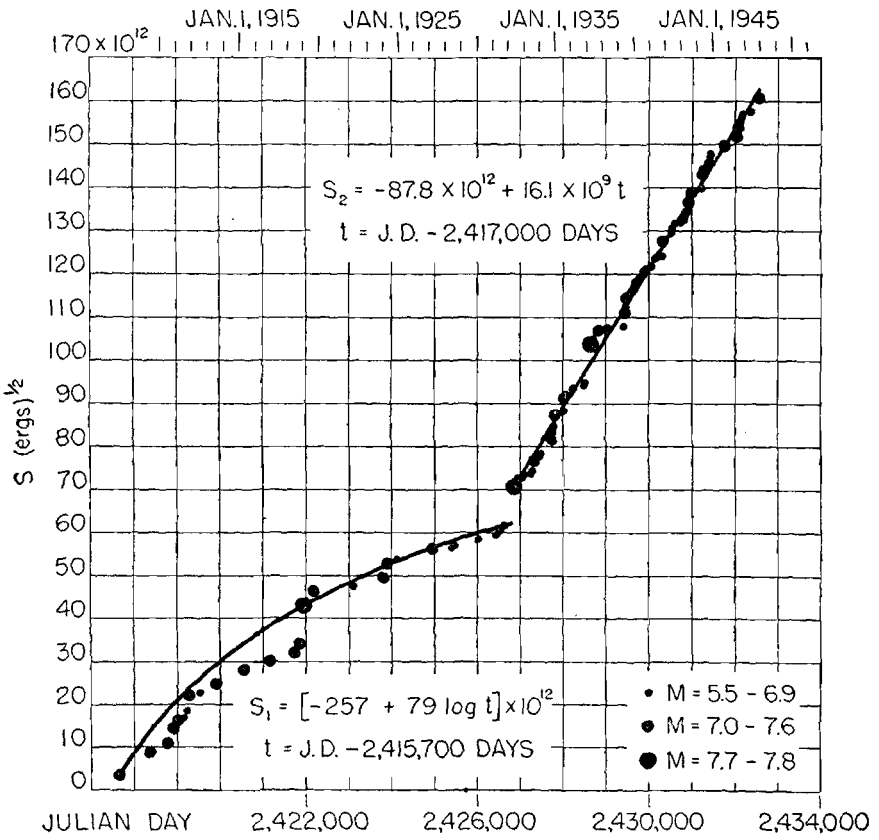

FIGURE 2.—STRAIN-REBOUND INCREMENTS OF TONGA-KERMADEC DEEP SEQUENCE (h = 70 — 480 km.) The plotted values are multiplied by the undetermined constant C of equation (5).

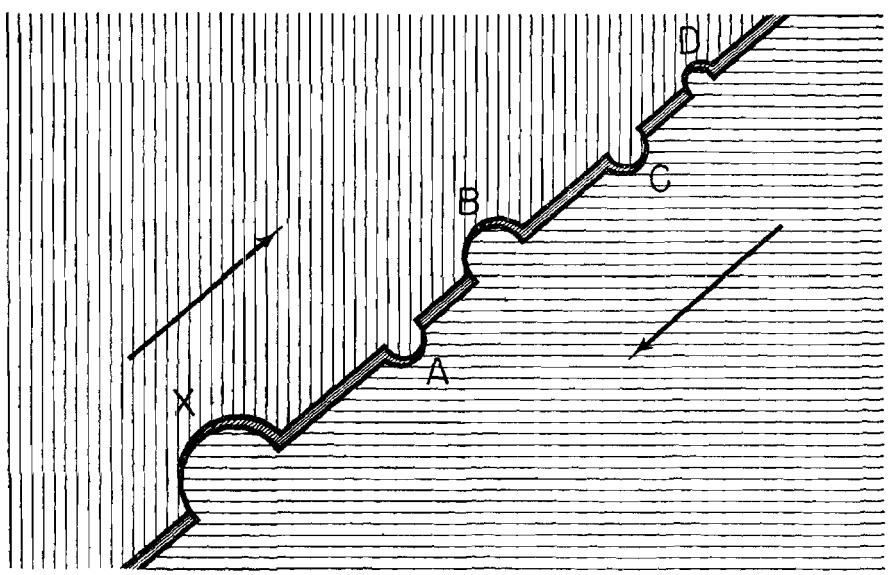

FIGURE 3.—TONGA-KERMADEC FAULT MECHANISM SUGGESTED BY STRAIN-REBOUND CURVE OF THE DEEP SEQUENCE

sequence earthquakes. In order to account for the shape of this first phase it must be assumed that one point X had a much higher locking strength than any of the others. At the time rapidly at a uniform rate with no further accumulation of strain. The graph for S_2 which represents this movement is therefore a straight line. The great shock of May 26, 1932, occurred

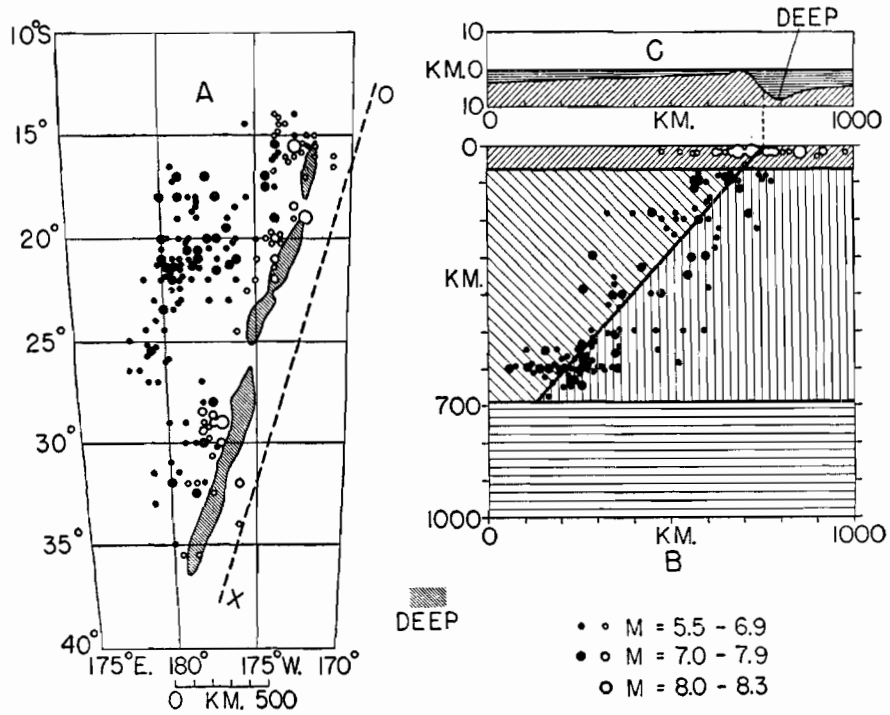

FIGURE 4.—TONGA-KERMADEC EARTHQUAKES AND OCEANIC DEEPS

The plane of the great fault intersects the earth's surface along the line of oceanic deeps. The slanting line in B represents the intersection of the fault with a vertical plane perpendicular to the line of oceanic deeps.

when the sequence began, faulting at the different minor points was frequent, and the block movements were rapid except in the vicinity of the major point X. The obstruction to the movements of the blocks presented by this point produced strain in the blocks which increased with time. As a result of this accumulating strain, the rate of movement of the blocks as well as the frequency of occurrence of the earthquakes decreased with time as shown by the graph of S_1. Finally on May 26, 1932, the stress at point X exceeded its locking strength, and this major obstruction gave way and thus generated the largest earthquake of the sequence. Thereafter movement of the blocks was resisted only by the minor surface irregularities, and consequently they proceeded at a depth of 600 km. Moreover it produced a series of aftershocks, seven of which were large enough to be recorded in Pasadena.

Since the curve for the shallow sequence (Fig. 1) bears no relationship to that of the deep sequence (Fig. 2) it may be concluded that there is no effective mechanical coupling between the two layers in which these sequences have their origins. Thus the boundary which separates them at a depth of approximately 70 km. must be a surface of profound discontinuity in the physical state or composition of the rock. The discontinuity in the seismic wave speed at this boundary appears to be quite small (Gutenberg, 1948). The absence of any term proportional to the time in equation (8) for S_1 indicates that although the layer, in

which this sequence originates, extends to a depth of nearly 700 km., the rock was able to maintain a stress without appreciable flow for 24 years.

Since the uncertainty in the location of the hypocenters in depth and geographical position can be indicated on the plane of the figure by a circle of approximately 100-km. radius it

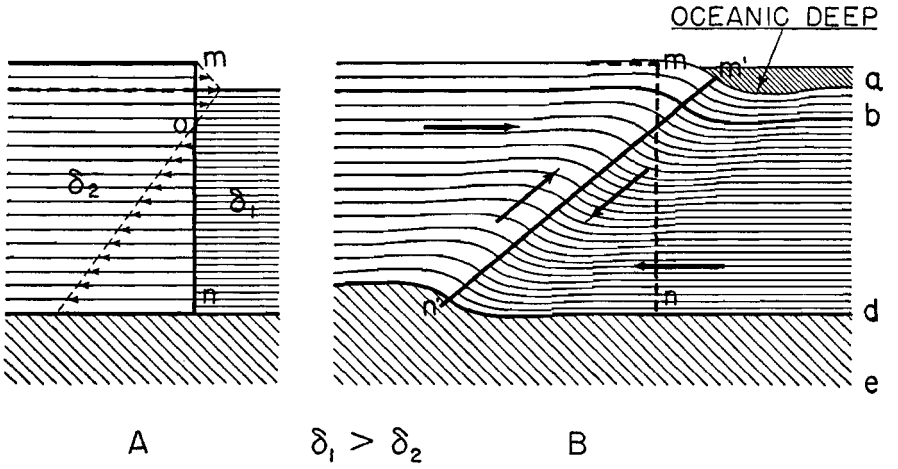

FIGURE 5.—SKETCH ILLUSTRATING PROPOSED ORIGIN OF THE GREAT TONGA-KERMADEC FAULT

A map of epicenters of the Tonga-Kermadec sequences is shown in Figure 4A. The neighboring oceanic deeps are also indicated. The epicenters of shallow-focus earthquakes are shown as open circles. while those of deep-focus shocks are represented by solid circles. Figure 4B represents a vertical section of the region taken perpendicular to the line OX which was drawn parallel to the trend of the oceanic deeps. The hypocenters corresponding to the epicenters of Figure 4A are shown projected horizontally on the section. In this drawing the vertical and horizontal scales are equal. The oceanic deeps are not shown since, to scale, their depth is about equal to the width of a line. Figure 4C represents an average profile of the upper 10 kilometers of the region, with the vertical scale exaggerated ten fold in order to show the oceanic deeps. The heavy horizontal line at the 70-km. depth represents the discontinuity between the shallow and deep layers. The heavy horizontal line at the 690 km. depth indicates the discontinuity between the seismically active deep layer and the layer below in which presumably secular strains of the kind that produce earthquakes do not or cannot exist. The heavy oblique line represents the average distribution of the projected foci. may be assumed that if the observational errors were small enough all the points would lie on or close to the line. Thus we may assume that the hypocenters determine an oblique fault having a plane surface indicated in the figure by the line, and that this is the fault determined by the strain-rebound curves. If the spread in the points is real they determine a fault zone which is still fairly narrow in comparison with its length. The fault plane cuts the earth's surface along the steep western slopes of the oceanic deeps (Fig. 4C). The total length of the fault as shown on the Map Figure 4A is approximately 2500 km. (1500 mi.). The transverse dimension measured along the oblique intersection is approximately 900 km. (540 mi.). This great fault is thus larger than any previously known active fault. A simple hypothesis as to its origin can be described with the help of Figure 5. Assume that originally a continental mass of density δ_2 was in contact along the surface mn with an oceanic mass of density δ_1 (Fig. 5A). As a result of secular flow in the rock masses a hydrostatic pressure $gh_1\delta_1$ developed at the depth h_1 within the oceanic mass, and a corresponding pressure $gh_2\delta_2$ developed at a depth h_2 within the continental mass. The constant g is the acceleration of

gravity. Thus at any given point on the contact surface *mn* the two pressures produced a differential stress, acting perpendicular to the boundary, given by their difference Δ, where

$$\Delta = (h_1\delta_1 - h_2\delta_2)g$$

A possible distribution with respect to depth of the differential stress Δ is represented on an arbitrary scale in the figure. The direction and distance of the arrows from the line *mn* indicate the direction and intensity of the stress. At the bottom of the deeper layer the differential stress was greatest and was directed toward the continental mass. It decreased linearly toward shallower depths as indicated by the light dashed line drawn through the arrow heads. At some level near the earth's surface the greater height h_2 of the continental mass relative to that of the oceanic mass h_1 offset its lower density, and the differential pressure was zero as at *O* in the figure. Above this level the hydrostatic pressure in the continental mass was greater than that in the denser oceanic mass, and the differential stress was therefore directed toward the oceanic mass. It passed through a secondary maximum at the level of the oceanic mass surface and fell to zero at the continental surface.

Acting over a sufficiently long interval of time this differential stress pattern produced a distortion of the two masses which resulted in a configuration such as shown in Figure 5B. Near the surface the continental mass flowed over the oceanic mass, while in the depths the oceanic mass pushed under the continental mass. Thus the originally vertical contact surface *mn* became the inclined surface *m'n'*. Below the level at which the differential pressure was zero the parallel component was directed downward on the oceanic side of the contact, and above this level it was directed upward on the continental side. Thus the parallel stress components transformed the contact into a fault in which the oceanic block moves downward and the continental block moves upward along the oblique fault plane. The surface distortions resulting from the faulting stresses are indicated in the figure. The downwarping of the oceanic block thus produced the depressions which form the oceanic deeps.

South American Earthquake Sequences

The observed data for the South American sequences are given in Tables 3, 4, and 5. A graph of *S* for the shallow-earthquake sequence is shown in Figure 6. For the period of time over which observations are available this graph is a straight line. On the basis of a single fault structure the straight line indicates that the fault block moves at a uniform rate.

Figure 7 is a graph of *S* for the intermediate depth sequence (*h=70–300 km.*) drawn on semilog co-ordinates. In this graph *S* takes the form of two intersecting straight lines. If plotted on arithmetic co-ordinates these lines would be exponential curves concave upward. They represent flows which increase exponentially with time. If these movements are produced in response to constant stresses acting on the fault rocks, they correspond to a type of creep which is characteristic of substances maintained in the annealing range of temperature above the strain-hardening limit. Since the rate of flow is curvilinear with respect to time and presumably with respect to stress it is defined as plastic flow. (A viscous flow is linear in relation to stress. The flow contribution in strain is not recovered upon release of stress.) On May 20, 1918, JD 2,421,734, the first phase ended. After an interval of $2\frac{1}{4}$ years the second phase began on August 13, 1920, with a reduced rate. Discontinuities of this type have been observed in a number of other sequences studied by the writer. Their cause remains obscure. They must represent sudden changes in stress, friction, or physical state of the fault masses. In any case it is difficult to understand how changes can occur throughout such large structures in such short intervals of time.

A graph of *S* plotted against time for the deep-focus sequence (*h=550–660 km.*) is shown in Figure 8. This graph takes the form of intersecting straight lines in linear co-ordinates, indicating constant velocity movements of the fault blocks. From the date at which observations began April 28, 1911, until January 17, 1922, the block velocity was large, and the earthquakes which determined it were large. After that interval the earthquake frequency increased appreciably, while the magnitudes

TABLE 3.—SOUTH AMERICAN SHALLOW SEQUENCE ($h < 70$ km.)

Date	J.D.	ϕ	λ	M	$J^{\frac{1}{2}} \times 10^{12}$	$S \times 10^{12}$
1906, Jan. 31	2,417,242	1 N	81½ W	8.6	55.0	55.0
1906, Aug. 17	17,440	33 S	72	8.4	35.0	90.0
1909, June 8	18,466	26½ S	70½	7.6	7.1	97.1
1911, Sept. 15	19,295	20 S	72	7.3	3.5	100.6
1913, July 28	19,977	17 S	74	7.0	2.0	102.6
1913, Aug. 6	19,986	17 S	74	7.75	9.5	112.1
1914, Jan. 30	20,163	35 S	73	7.6	7.1	119.2
1917, Feb. 15	21,275	30 S	73	7.0	2.0	121.2
1917, July 27	21,437	31 S	70	7.0	2.0	123.2
1917, Aug. 31	21,470	4 N	74	7.3	3.5	126.7
1918, Dec. 4	21,932	26 S	71	7.75	9.5	136.2
1920, Jan. 30	22,354	3 N	77½	6.0	.2	136.4
1920, Aug. 3	22,540	27½ S	70	6.75	1.2	137.6
1920, Sept. 24	22,592	6 N	83	6.5	.7	138.3
1922, Jan. 6	23,061	16½ S	73	7.2	3.2	141.5
1922, Oct. 11	23,339	16 S	72½	7.4	4.5	146.0
1922, Nov. 7	23,366	28 S	72	7.0	2.0	148.0
1922, Nov. 11	23,368	28½ S	70	8.3	28.0	176.0
1923, May 4	23,544	28¾ S	71¾	7.0	2.0	178.0
1924, Mar. 11	23,856	4 S	82	6.75	1.2	179.2
1924, June 22	23,959	5½ N	78½	6.5	.7	179.9
1924, Oct. 18	24,077	2½ N	80	6.75	1.2	181.1
1925, May 15	24,286	26 S	71½	7.1	2.5	183.6
1926, Aug. 12	2,424,740	23 S	70 W	6.75	1.2	184.8
1927, Mar. 13	24,953	6 S	81½	6.0	.2	185.0
1927, Aug. 20	25,113	5 N	82½	7.0	2.0	187.0
1927, Nov. 14	25,199	30½ S	71½	6.75	1.2	188.2
1928, Apr. 9	25,346	13 S	69½	6.9	1.6	189.8
1928, Apr. 27	25,364	13 S	69½	6.75	1.2	191.0
1928, May 14	25,381	5 S	78	7.3	3.5	194.5
1928, July 18	25,446	5½ S	79	7.0	2.0	196.5
1928, July 28	25,456	31 S	71	6.5	.7	197.2
1928, Nov. 20	25,561	22½ S	70½	7.1	2.5	199.7
1928, Dec. 1	25,572	35 S	72	8.0	16.0	215.7
1929, May 30	25,762	35 S	68	6.75	1.2	216.9
1929, Aug. 15	25,839	5 N	83½	6.5	.7	219.6
1930, Dec. 24	26,335	25 S	66	6.0	.2	217.8
1931, Mar. 18	26,419	32½ S	72	7.1	2.5	220.3
1931, Apr. 3	26,435	9¼ S	79	6.25	.4	220.7
1931, May 20	26,482	27½ S	71½	6.25	.4	221.1
1931, June 15	26,508	14½ S	75½	6.0	.2	221.3
1931, June 29	26,522	29½ S	71	6.0	.2	221.5
1931, Sept. 12	26,597	5 N	77½	6.25	.4	221.9
1932, Sept. 5	26,956	6 S	81	6.0	.2	222.1
1933, Feb. 23	27,127	20 S	71	7.6	7.1	229.2
1933, May 6	27,199	5½ N	83	6.5	.7	229.9
1933, May 6	2,427,199	5¾ N	82¾ W	6.0	.2	230.1
1933, Oct. 2	27,348	2 S	81	6.9	1.6	231.7
1933, Oct. 3	27,349	1¾ S	80¾	6.25	.4	232.1
1933, Oct. 3	27,349	1¾ S	80¾	6.0	.2	232.3
1934, Apr. 3	27,531	4 N	78	6.0	.2	232.5
1934, Aug. 6	27,656	3¼ N	77¾	6.0	.2	232.7

TABLE 3.—*Continued*

Date	J.D.	ϕ	λ	M	$J^{\frac{1}{2}} \times 10^{12}$	$S \times 10^{12}$
1935, June 28	2,427,982	34 S	73	6.0	.2	232.9
1935, Aug. 5	28,021	35 S	72	6.0	.2	233.1
1935, Dec. 24	28,161	3 N	79	6.75	1.2	234.3
1936, May 22	28,311	32 S	66	6.0	.2	234.5
1936, July 13	28,363	24½ S	70	7.3	3.5	238.0
1936, July 26	28,376	24 S	70	6.75	1.2	239.2
1937, March 14	28,607	24½ S	69½	6.5	.7	239.9
1937, June 21	28,706	8½ S	80	6.75	1.2	241.1
1937, July 8	28,723	3 N	84	6.0	.2	241.3
1937, Dec. 12	28,880	25 S	70	6.0	.2	241.5
1937, Dec. 24	28,893	10½ S	76½	6.25	.4	241.9
1938, Apr. 17	29,016	19 S	69½	6.5	.7	242.6
1939, Sept. 20	29,527	11½ S	75½	6.0	.2	242.8
1940, March 31	29,720	19 S	70½	6.0	.2	243.0
1940, Apr. 8	29,728	33½ S	71½	6.0	.2	243.2
1940, May 5	29,755	7 S	80	6.0	.2	243.4
1940, May 24	29,774	10½ S	77	8.0	16.0	259.4
1940, Oct. 6	2,429,909	22 S	71 W	6.75	1.2	260.6
1941, July 3	30,179	31½ S	69½	6.25	.4	261.0
1941, July 11	30,187	5 N	82½	6.25	.4	261.4
1942, May 14	30,525	¾ S	81½	7.9	13.0	274.4
1942, Aug. 24	30,596	15 S	76	8.1	20.0	294.4
1942, Oct. 8	30,641	6 N	82¾	6.0	.2	294.6
1943, Mar. 5	30,789	5¼ N	82½	6.75	1.2	295.8
1943, Apr. 6	30,821	30¾ S	72	7.9	13.0	308.8
1943, May 22	30,867	30¾ S	72	6.75	1.2	310.0
1943, July 5	30,911	16 S	74	6.75	1.2	311.2
1944, Jan. 15	31,095	31¼ S	68¾	7.4	4.5	315.7
1944, Oct. 23	31,387	½ N	80½	6.9	1.6	317.3
1946, Aug. 2	32,035	26½ S	70½ W	7.5	5.6	322.9
1946, Nov. 10	32,135	8½ S	77½	7.25	3.4	326.3
1947, Nov. 1	32,491	10½ S	75	7.3	3.5	329.8

decreased sufficiently to reduce the block velocity to 0.22 of its initial value. There is some indication that in January 1946 the initial rate of the blocks was resumed, but more time will be required to settle this question. It is noteworthy that the discontinuity in this deep sequence occurred very nearly at the same time that the intermediate-sequence discontinuity occurred and that in each the rate decreased. This would indicate that a certain amount of mechanical coupling exists between the two layers in which these sequences have their origins. On the other hand there is no evidence of coupling between the shallow and intermediate layers. The boundary between them must represent a profound mechanical discontinuity similar to the corresponding boundary in the Tonga-Kermadec region. Possibly, since the shallow sequences generally show greater strain-rebound movements than the deeper sequences, the shallow movements may include movements coupled with the deeper layers along with horizontal or other movements which are independent of them. On this basis, however, we would expect to observe some effect of the lower-layer velocity discontinuities on the surface-layer movements, unless the movements in the two layers are complementary. These effects appear to be lacking in both the Tonga-Kermadec region and in South America. There is some evidence that faulting in the shallow layers of both these regions is principally horizontal. Nevertheless these layers are sufficiently thin in relation to the thick-

TABLE 4.—SOUTH AMERICAN INTERMEDIATE SEQUENCE (h = 70–300 km.)

Date	J.D.	ϕ	λ	M	$J^{\frac{1}{2}} \times 10^{13}$	$S \times 10^{13}$	h
1906, Sept. 28	2,417,482	2 S	79 W	7.5	5.6	5.6	150
1909, May 17	18,444	20 S	64 W	7.1	2.5	8.1	250
1910, Oct. 4	18,949	22 S	69 W	7.25	3.4	11.5	120
1914, Feb. 26	20,190	18 S	67 W	7.2	3.2	14.7	130
1915, June 6	20,655	18½ S	68½ W	7.6	7.1	21.8	160
1916, Aug. 25	21,101	21 S	68 W	7.5	5.6	27.4	180
1918, May 20	21,734	28½ S	71½ W	7.5	5.6	33.0	80
1920, Aug. 13	22,612	20 S	68 W	6.5	.7	33.7	150
1921, Oct. 20	22,983	18½ S	68 W	7.0	2.0	35.7	120
1922, Mar. 28	23,142	21 S	68 W	7.2	3.2	38.9	90
1923, Sept. 2	23,665	16 S	68½ W	7.0	2.0	40.9	150
1924, July 22	23,989	2 S	80 W	6.5	.7	41.6	250
1925, Jan. 5	24,156	14 S	73½ W	6.5	.7	42.3	200
1925, June 7	24,309	3 N	78 W	6.75	1.2	43.5	170
1925, June 23	24,325	0	77 W	6.75	1.2	44.7	180
1926, Mar. 7	24,582	5 S	76½ W	6.5	.7	45.4	150
1926, Apr. 28	24,634	24 S	69 W	7.0	2.0	47.4	180
1927, Apr. 14	24,985	32 S	69½ W	7.1	2.5	49.9	110
1927, May 22	25,023	21 S	67 W	6.25	.4	50.3	140
1927, Aug. 1	25,094	24 S	66½ W	6.5	.7	51.0	200
1927, Oct. 3	25,157	21 S	68 W	6.5	.7	51.7	100
1927, Nov. 26	25,211	24½ S	67 W	6.75	1.2	52.9	180
1928, May 26	25,393	23½ S	69 W	6.25	.4	53.3	130
1928, Sept. 21	2,425,501	15 S	70½ W	6.75	1.2	54.5	250
1929, May 25	25,757	8½ S	75½ W	6.75	1.2	55.7	150
1929, Oct. 19	25,904	23 S	69 W	7.5	5.6	61.3	100
1929, Oct. 19	25,904	23 S	69 W	6.0	.2	61.5	100
1930, Sept. 23	26,243	26 S	66 W	6.5	.7	62.2	150
1930, Nov. 24	26,305	2 S	77 W	6.25	.4	62.6	100
1931, Apr. 3	26,435	27 S	65 W	6.25	.4	63.0	180
1931, May 28	26,490	20½ S	70½ W	6.5	.7	63.7	120
1931, July 11	26,534	8½ S	74½ W	6.25	.4	64.1	120
1931, July 18	26,541	22½ S	69 W	6.75	1.2	65.3	150
1932, Jan. 20	26,727	12 S	77½ W	6.75	1.2	66.5	100
1932, Apr. 26	26,824	25 S	69½ W	6.5	.7	67.2	70
1932, June 18	26,877	20 S	71 W	6.25	.4	67.6	70
1932, July 29	26,918	19 S	70 W	6.0	.2	67.8	110
1932, Nov. 1	27,013	24 S	70 W	6.0	.2	68.0	100
1932, Nov. 29	27,041	32 S	71 W	6.75	1.2	69.2	110
1932, Dec. 9	27,051	15 S	75 W	6.5	.7	69.9	75
1933, July 23	27,277	15¾ S	75¼ W	6.0	.2	70.1	80
1933, July 31	27,285	15½ S	75½ W	6.0	.2	70.3	80
1933, Aug. 6	27,291	11 S	75½ W	6.5	.7	71.0	100
1933, Aug. 9	27,294	15½ S	68½ W	6.25	.4	71.4	170
1933, Oct. 1	27,347	7 S	75¼ W	6.25	.4	71.8	120
1933, Oct. 12	27,358	23 S	69½ W	6.25	.4	72.2	100
1933, Oct. 25	2,427,371	23.0 S	66.7 W	7.0	2.0	74.2	220
1933, Nov. 14	27,391	32 S	69½ W	6.5	.7	74.9	110
1933, Dec. 21	27,398	31 S	69 W	6.25	.4	75.3	120
1934, June 11	27,600	33½ S	64½ W	6.0	.2	75.5	100
1934, June 11	27,600	33½ S	64½ W	6.0	.2	75.7	100
1934, June 24	27,613	22.0 S	68.6 W	6.9	1.6	77.3	100

TABLE 4.—*Continued*

Date	J.D.	ϕ	λ	M	$J^{\frac{1}{2}} \times 10^{12}$	$S \times 10^{12}$	h
1934, Oct. 29	2,427,740	5 S	78 W	6.25	.4	77.7	110
1934, Dec. 4	27,775	19½ S	69½ W	6.9	1.6	79.3	130
1934, Dec. 16	27,787	24 S	68 W	6.0	.2	79.5	150
1934, Dec. 23	27,794	21 S	68 W	6.5	.7	80.2	100
1935, Feb. 13	27,847	25½ S	69 W	6.5	.7	80.9	100
1935, Feb. 28	27,862	23 S	67 W	6.25	.4	81.3	200
1935, Mar. 8	27,870	4 S	80 W	6.0	.2	81.5	100
1935, Mar. 26	27,888	15½ S	73 W	6.0	.2	81.7	120
1935, Sept. 18	28,064	5½ N	76 W	6.25	.4	82.1	80
1935, Sept. 19	28,065	15½ S	70 W	6.5	.7	82.8	250
1935, Nov. 2	28,109	2 S	79 W	6.0	.2	83.0	130
1936, Apr. 30	28,289	31 S	65 W	6.0	.2	83.2	200
1936, May 6	28,295	8 S	75 W	6.0	.2	83.4	160
1936, June 22	28,342	22 S	68 W	6.0	.2	83.6	100
1936, July 4	28,354	18 S	70 W	6.0	.2	83.8	140
1936, Nov. 7	28,480	23 S	67 W	6.0	.2	84.0	200
1936, Nov. 29	28,502	22½ S	67 W	6.0	.2	84.2	230
1936, Dec. 5	28,508	20 S	70½ W	6.0	.2	84.4	100
1937, Mar. 19	2,428,612	29 S	70 W	6.0	.2	84.6	70
1937, Mar. 29	28,622	15½ S	71 W	6.75	1.2	85.8	120
1937, May 21	28,675	2½ N	77½ W	6.5	.7	86.5	90
1937, July 9	28,724	16 S	72 W	6.0	.2	86.7	180
1937, July 19	28,734	1½ S	76½ W	7.1	2.2	88.9	190
1937, Sept. 24	28,801	22½ S	70 W	6.0	.2	89.1	130
1937, Oct. 12	28,819	25 S	68½ W	6.5	.7	89.8	110
1937, Oct. 27	28,834	34½ S	71 W	6.0	.2	90.0	110
1938, Jan. 16	28,915	6 S	75 W	6.0	.2	90.2	100
1938, Feb. 5	28,935	4½ N	76¼ W	7.0	2.0	92.2	160
1938, Apr. 24	29,013	23½ S	66 W	6.0	.2	92.4	180
1938, June 15	29,065	31 S	70½ W	6.0	.2	92.6	70
1938, June 23	29,073	30½ S	70 W	6.5	.7	93.3	70
1938, Aug. 4	29,115	24 S	68 W	6.75	1.2	94.5	220
1939, Jan. 18	29,292	29½ S	71 W	6.25	.4	94.9	70
1939, Apr. 18	29,372	27 S	70½ W	7.4	4.5	99.4	100
1939, Apr. 25	29,379	12½ S	75½ W	6.25	.4	99.8	150
1939, May 19	29,403	18 S	69 W	6.25	.4	100.2	100
1939, July 4	29,449	21 S	66 W	6.75	1.2	101.4	290
1939, Oct. 5	29,542	22 S	67 W	6.0	.2	101.6	240
1939, Oct. 7	29,544	18½ S	70 W	6.0	.2	101.8	110
1940, Feb. 12	29,672	26½ S	71 W	6.5	.7	102.5	70
1940, Aug. 7	29,849	22 S	68½ W	6.25	.4	102.9	110
1940, Aug. 26	29,868	11½ S	75 W	6.0	.2	103.1	110
1940, Sept. 18	2,429,891	23 S	68 W	6.5	.7	103.8	110
1940, Sept. 29	29,902	35 S	70 W	6.25	.4	104.2	110
1940, Oct. 1	29,904	30 S	72½ W	6.5	.7	104.9	80
1940, Oct. 3	29,906	21 S	70 W	6.25	.4	105.3	110
1940, Oct. 4	29,907	22 S	71 W	7.3	3.5	108.8	75
1940, Oct. 23	29,926	2 S	76 W	6.0	.2	109.0	140
1940, Oct. 24	29,927	35 S	72½ W	6.75	1.2	110.2	80
1940, Dec. 22	29,986	15½ S	68½ W	7.1	2.5	112.7	230
1941, Jan. 24	30,019	3¼ S	76¾ W	6.5	.7	113.4	120
1941, Apr. 3	30,088	22½ S	66 W	6.5	.7	114.1	260

TABLE 4.—*Continued*

Date	J.D.	ϕ	λ	M	$J^{\frac{1}{2}} \times 10^{12}$	$S \times 10^{12}$	h
1941, Apr. 3	2,430,088	22½ S	66 W	7.2	3.2	117.3	260
1941, July 10	30,186	18½ S	70 W	6.0	.2	117.5	120
1941, Aug. 14	30,221	23 S	66¾ W	6.0	.2	117.7	180
1941, Sept. 18	30,256	13¾ S	72½ W	7.0	2.0	119.7	100
1941, Oct. 15	30,283	15½ S	74 W	6.0	.2	119.9	110
1941, Nov. 10	30,309	22 S	67 W	6.25	.4	120.3	200
1942, June 29	30,540	32 S	71 W	6.9	1.6	121.9	100
1942, July 8	30,549	24 S	70 W	7.0	2.0	123.9	140
1942, Nov. 6	30,670	6 S	77 W	6.75	1.2	125.1	130
1943, Jan. 30	30,755	2 S	80½ W	6.9	1.6	126.7	100
1943, Feb. 16	30,772	15 S	72 W	7.0	2.0	128.7	190
1943, Mar. 14	30,798	20 S	69½ W	7.2	3.2	131.9	150
1943, Apr. 5	2,430,820	6½ S	76 W	6.5	.7	132.6	140
1943, Nov. 29	31,058	29½ S	68½ W	6.75	1.2	133.8	100
1943, Dec. 1	31,060	21 S	69 W	7.25	3.4	137.2	100
1943, Dec. 22	31,081	2½ S	77 W	6.25	.4	137.6	130
1944, Feb. 29	31,150	14½ S	70½ W	7.0	2.0	139.6	200
1944, May 9	31,220	2½ N	75½ W	6.0	.2	139.8	100
1944, July 23	31,295	24 S	66½ W	6.0	.2	140.0	250
1944, Dec. 22	31,447	25 S	70 W	6.5	.7	140.7	120
1945, July 9	31,646	2½ N	76½ W	6.5	.7	141.4	100
1945, Aug. 21	31,689	10½ S	75 W	6.75	1.2	142.6	120
1945, Sept. 13	31,712	33¼ S	70½ W	7.1	2.5	145.1	100
1946, July 26	32,028	19¾ S	70½ W	6.75	1.2	146.3	70
1946, Sept. 30	32,094	13 S	76 W	7.0	2.0	148.3	70

TABLE 5.—SOUTH AMERICA DEEP SEQUENCE (h = *550–660 km.*)

Date	J.D.	ϕ	λ	M	$J^{\frac{1}{2}} \times 10^{12}$	$S \times 10^{12}$	h
1911, Apr. 28	2,419,156	0 S	71 W	7.1	2.50	2.50	600
1912, Dec. 7	19,746	29	62½	7.5	5.60	8.10	620
1915, Apr. 23	20,613	8	68	7.25	3.30	11.40	650
1916 June 21	21,038	28½	63	7.5	5.60	17.00	600
1921, Dec. 18	23,044	2½	71	7.6	7.10	24.10	650
1922, Jan. 17	23,073	2½	71	7.6	7.10	31.20	650
1922, July 10	23,247	19	62	6.75	1.20	32.40	630
1922, Sept. 4	23,303	10½	69½	6.9	1.60	34.00	660
1926, Feb. 9	24,557	29	62	6.5	.70	34.70	660
1927, Apr. 6	24,979	10	70	6.0	.25	34.95	600
1928, Jan. 5	25,253	19½	64	6.75	1.20	36.15	640
1928, Aug. 15	25,466	28	62½	6.50	.70	36.85	620
1930, Aug. 4	26,194	9½	70½	6.50	.70	37.55	650
1933, Aug. 29	27,310	10.9	69.5	6.50	.70	38.25	650
1934, Jan. 9	27,448	28½	63	6.0	.25	38.50	630
1935, Dec. 14	28,152	9½	70½	6.9	1.60	40.10	650
1935, Dec. 16	28,155	9½	70½	6.25	.42	40.52	600
1935, Dec. 28	28,167	9½	70½	5.75	.15	40.67	650
1936, Jan. 14	28,183	29	62½	6.9	1.60	42.27	620
1939, Jan. 24	29,289	26½	63	6.0	.25	42.52	580
1939, Dec. 4	29,623	6½	70	5.5	.10	42.62	600
1940, May 1	29,751	25½	62½	6.25	.42	43.04	580
1940, Sept. 23	2,429,896	23 S	64 W	6.5	.70	43.74	550
1940, Sept. 24	29,897	9½	70½	6.0	.25	43.99	600
1942, Nov. 30	30,694	27	63½	6.5	.70	44.69	590
1944, June 8	31,250	10	71	6.25	.42	45.11	600
1946, Aug. 28	32,061	26	63	7.20	3.20	48.31	580
1947, Jan. 29	32,215	26	63	7.25	3.30	51.61	580
1947, Aug. 6	32,404	9	72	6.75	1.20	52.81	600

ness of the deeper layers that they can take on the vertical warping produced by the vertically oblique faulting of these larger deep structures even though their own faulting movement may not conform with those of the deeper faults.

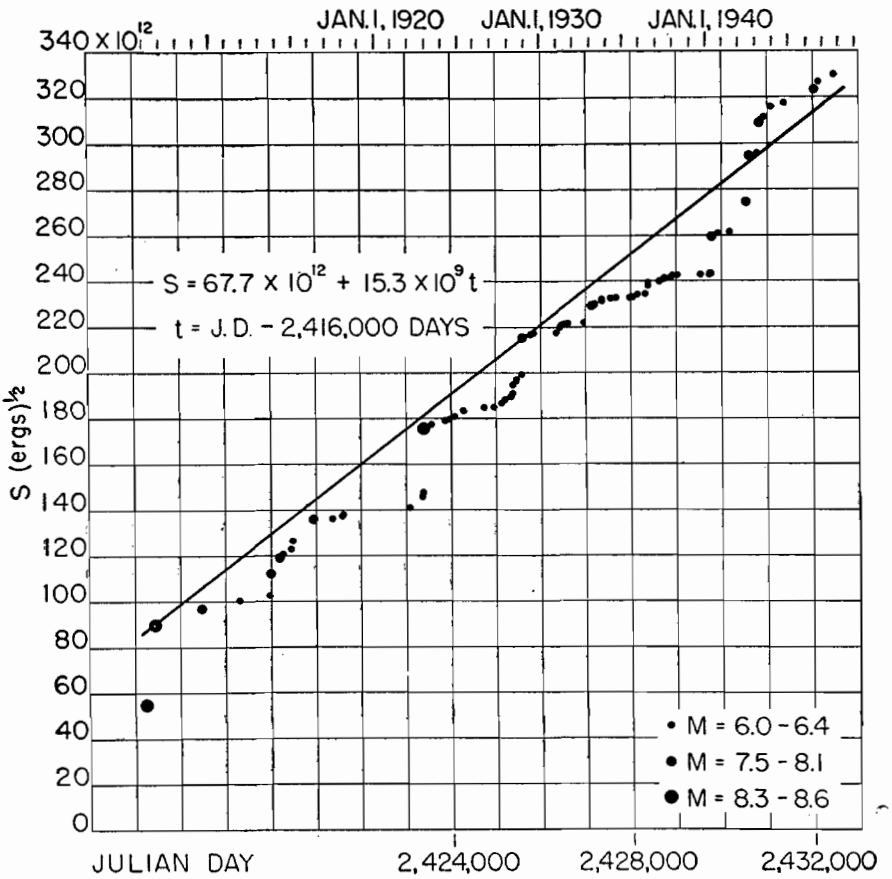

FIGURE 6.—STRAIN-REBOUND INCREMENTS OF THE SOUTH AMERICAN SHALLOW SEQUENCE (h < 70 km.) The plotted values are multiplied by the undetermined constant C of equation (5).

In Figure 9 the deep-focus sequence consists of two groups of epicenters centered roughly at 5° and 25° latitude south, respectively. Each group has the same number of shocks and in addition the same number in each indicated magnitude range. Thus although they represent areas of the fault block which are some 2000 km. apart their movements are very nearly identical. In the initial phase of this sequence (Fig. 8) the fault locked strongly following the fourth earthquake, and no additional earthquakes occurred for 5½ years. During this interval the strain continued to accumulate at the initial constant rate so that when the fault did give way it generated two great earthquakes which brought the total elastic-rebound movement to the value determined by the initial line. Thus for a period of 5½ years the rock of this fault maintained a linear elastic strain without flow at a depth of 650 kilometers. Clearly any remaining doubts as to the solidity of rocks at such depths must be abandoned.

A map of the region of the South American sequences is shown in Figure 9. Epicenters of shallow-focus earthquakes are shown as open circles. Those of intermediate-depth foci are shown as solid circles, and the deep-focus epi-

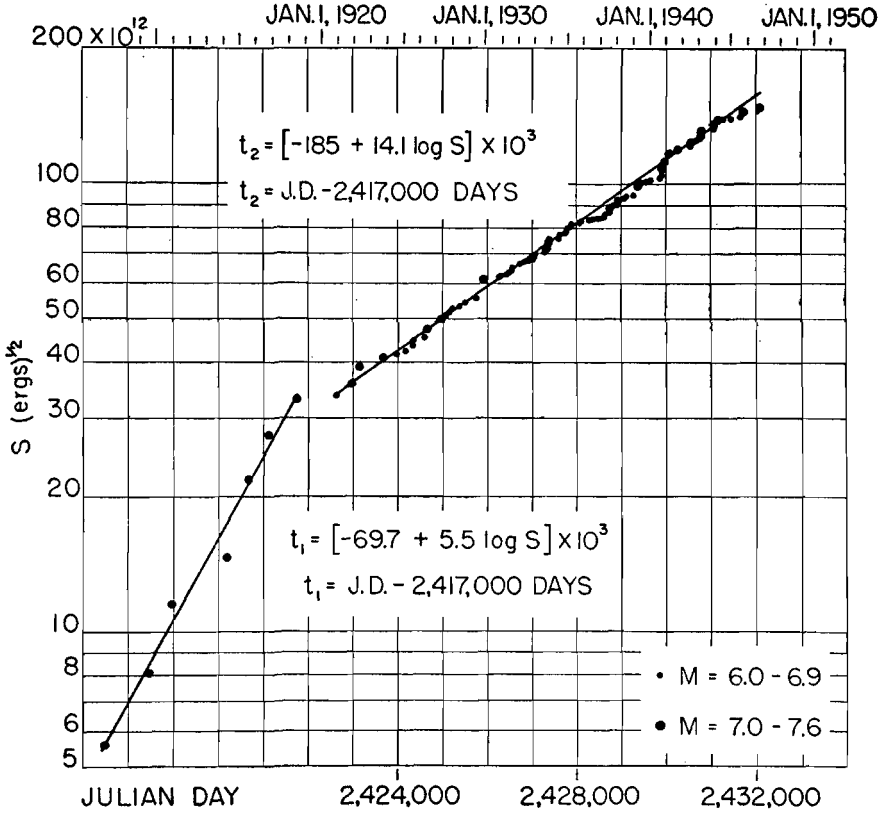

FIGURE 7.—STRAIN-REBOUND INCREMENTS OF THE SOUTH AMERICAN INTERMEDIATE SEQUENCE (h = 70 — 300 km.)
The plotted values are multiplied by the undetermined constant C of equation (5).

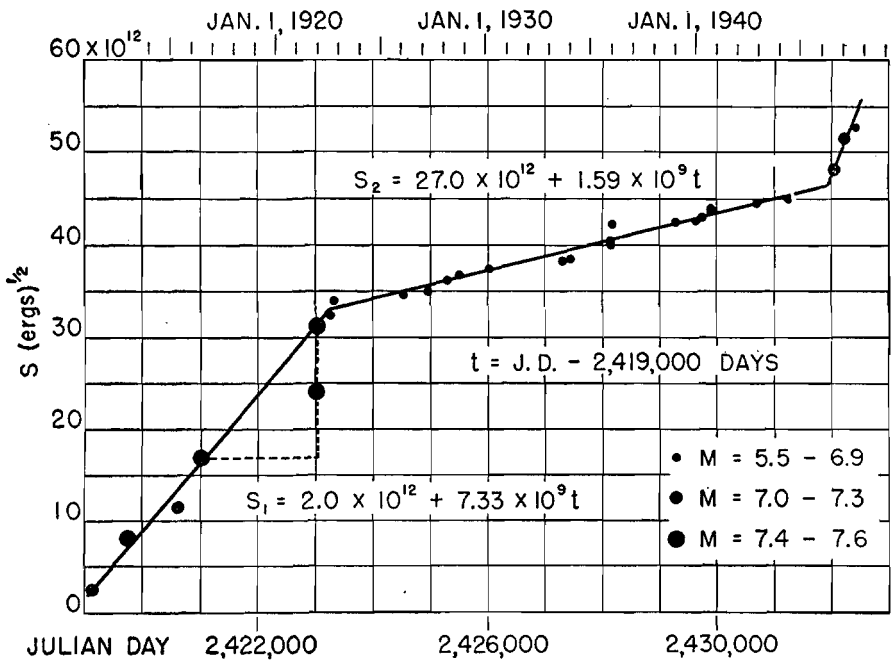

FIGURE 8.—STRAIN-REBOUND INCREMENTS OF THE SOUTH AMERICAN DEEP SEQUENCE (h = 550 — 660 km.)
The plotted values are multiplied by the undetermined constant C of equation (5).

centers are represented by triangles. The magnitude ranges of the earthquakes corresponding to the epicenters are indicated. The oceanic deeps are sketched in roughly. In this region which were drawn parallel to the neighboring deeps. Above each section is drawn an average profile of the upper 10 km. of the projected region of each section outlined by the dashed

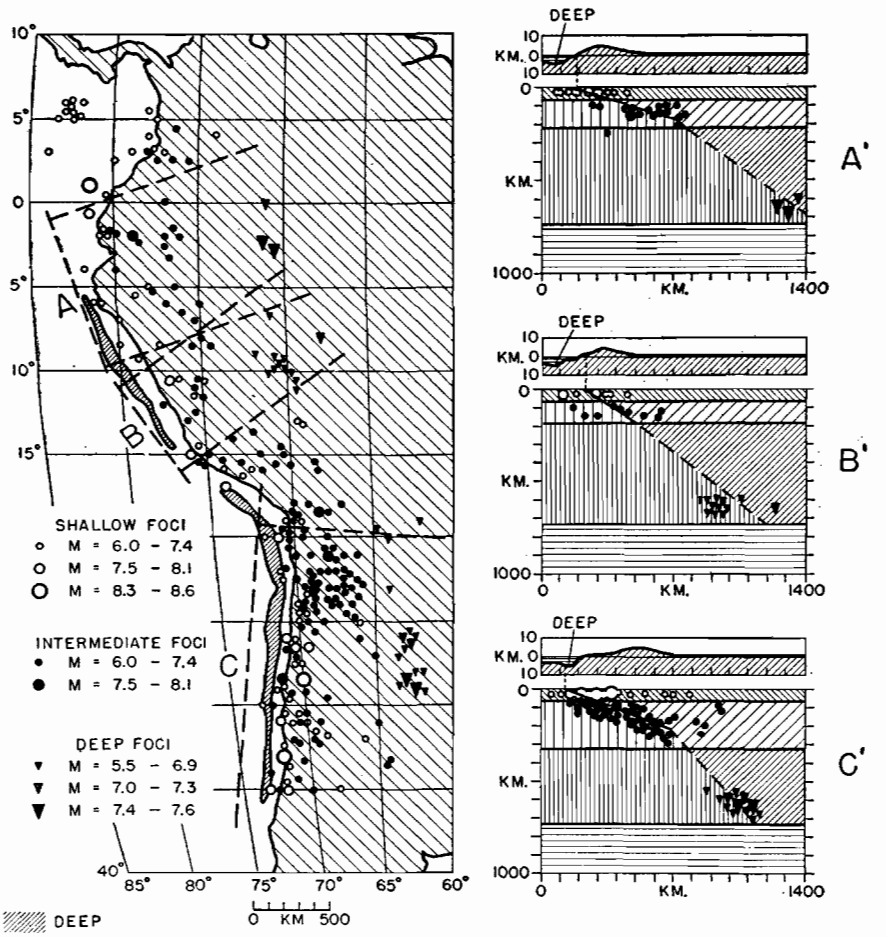

FIGURE 9.—SOUTH AMERICAN EARTHQUAKES AND OCEANIC DEEPS

The great fault intersects the earth's surface along the curved line of oceanic deeps. Its positions below the surface are indicated in the three sectional drawings A′, B′ and C′.

they have depths in excess of 8 km. Unlike the Tonga-Kermadec fault, the surfaces of this fault do not form a single plane. They can be thought of as a plane which has been bent and somewhat twisted along the long axis and bent along the short axis near the middle. It was necessary to make three sectional projections in order to display the three-dimensional distribution of the foci. Thus A', B', and C′ are the three vertical sections taken perpendicular to the lines A, B, and C respectively of the map parallel lines on the map. In these profiles the vertical scale is 10 times that of the horizontal scale. In this region the observational uncertainty in the position of the hypocenters is about 100 km. in any spatial direction. It may be assumed therefore that the lines drawn through the projected positions of the hypocenters in A', B', and C' (Fig. 9) represent the projections of the fault surface. The hypocenters in this region are not distributed uniformly with respect to depth as they are in the Tonga-Ker-

madec area. North of Lat. 15½°S. the intermediate-depth foci form a continuous distribution over the depth range 70–200 km. South of Lat. 15½°S. the continuous distribution ends at a depth of 300 km. There are no foci in the depth range 300–600 km. The deep foci occur only at a depth of 550 to 660 km. The origin of this fault may be explained on the basis of an original configuration such as the one shown at *A* (Fig. 10) in which the continental mass had three layers and the oceanic mass two (or three) layers of different density. Thus δ_1 was greater than δ_2, and δ_3 was greater than δ_4. The constants δ_1 and δ_3 may have been equal. In any case the inequality between δ_1 and δ_2 must have been greater than that between δ_3 and δ_4 to provide for the shallower slope of the fault in the 70–300 km. depth range. To account for the bend in the long axis of the fault it may be assumed that the inequality between δ_1 and δ_2 varied along the length of the fault; it was greatest north of Lat. 15½°S. and approximately constant south of that parallel of latitude. The inequalities in densities may have been due in part to temperature differences resulting from different rates of generation of radioactive heat energy. The total length of the fault is approximately 4500 km. (2700 mi.). Its transverse dimension which dips under the continent is approximately 900 km., and it extends to a depth of approximately 690 km.—more than one tenth of the radius of the earth. The long line of oceanic deeps which parallel the western coast of the continent was formed by the downwarping of the oceanic block of this great fault, and the upwarping of its continental block produced the Andes Mountains.

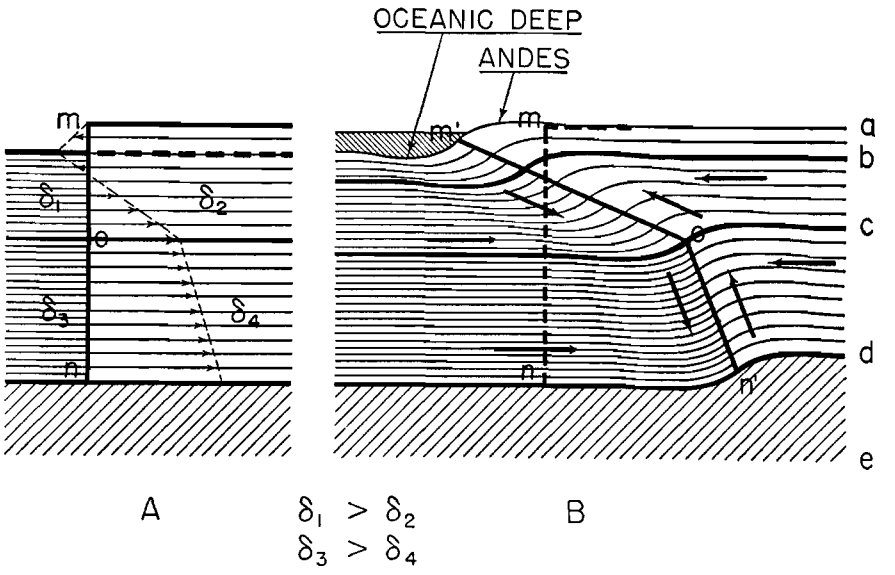

FIGURE 10.—SKETCH ILLUSTRATING PROPOSED ORIGIN OF THE GREAT SOUTH AMERICAN FAULT

OTHER DEEP-FOCUS SEQUENCES

A preliminary examination of a number of other deep-focus earthquake sequences which are associated with oceanic deeps indicates that they may all be generated on great faults similar to those described in this paper. Among these may be mentioned the Aleutian sequence, another one which extends from Southern Japan to Kamchatka, several sequences in the East Indies, the Central American sequences, and the West Indies sequences.

TSUNAMIS AND THE GREAT FAULTS

The characteristic movements of the great faults involve fairly large vertical components. It may be assumed, therefore, that a seismic sea wave or tsunami is generated whenever an earthquake focus on one of these faults is suffi-

ciently shallow to allow the faulting movement to reach the upper surfaces of the fault blocks where it can effect a sudden vertical displacement of the ocean floor. Moreover, the epicenter does not necessarily have to be situated within the areas of the oceanic deeps, since faulting or strain adjustment can be propagated up to several hundred kilometers from the focus. The faulting speed is finite and somewhat less than that of seismic waves (Benioff, 1938). Consequently the faulting impulse may arrive at the ocean floor up to several minutes after the beginning of the earthquake. The time of origin of the tsunami may thus be delayed with respect to the origin time of the earthquake. The sea waves generated by the upward movement of the oceanic block must begin with a rise in the water level, whereas those generated by the downward movement of the continental block must begin with a recession. Since the area of the ocean floor over the oceanic block is generally greater than that over the continental block the initial wave of recession is larger than the initial wave of advance. To an observer on the oceanic side of the fault all tsunamis would begin with a recession. On the other hand, to an observer on the continental side, the initial wave of advance may be so small as to be unnoticed, and the tsunami would thus appear to begin with a recession also. Presumably this accounts for the fact that most tsunamis are observed to begin with recessions.

References Cited

Benioff, Hugo (1938) *The determination of the extent of faulting with application to the Long Beach earthquake*, Seismol. Soc. Am., Bull., vol. 28, p. 77–84.

Griggs, David 2939) *The creep of rocks*, Jour. Geol., vol. 67, p. 25–251.

Gutenberg, Beno (1945) *Magnitude determination for deep-focus earthquakes*, Seismol. Soc. Am., Bull., vol. 35, p. 117.

——— (1948) *On the layer of relatively low wave velocity at a depth of about 80 kilometers*, Seismol. Soc. Am., Bull., vol. 38, p. 121–167.

——— and Richter, C. F. (1942) *Earthquake magnitude, intensity, energy, and acceleration*, Seismol. Soc. Am., Bull., vol. 32, p. 143–191.

——— —— ——— (1949) *Seismicity of the Earth*, Princeton Univ. Press.

Lutts, C. E., and Himmelfarb, David (1940) *The creep phenomenon in ropes and cords*, Am. Soc. Test. Mat., Pr., vol. 40, p. 1251.

Richter, C. F. (1935) An instrumental magnitude scale, Seismol. Soc. Am., Bull., vol. 25, p. 1–32.

Seismological Laboratory, 220 N. San Rafael Ave., Pasadena, Calif.

Manuscript Received by the Secretary of the Society, July 8, 1949

Publications of the Division of Geological Sciences, California Institute of Technology, Pasadena, Calif. Contribution No. 505